Precise Tip Positioning of a Flexible Manipulator Using Resonant Control

Iskandar A. Mahmood, S. O. Reza Moheimani, *Senior Member, IEEE*, and Bharath Bhikkaji

***Abstract*—A single-link flexible manipulator is fabricated to represent a typical flexible robotic arm. This flexible manipulator is modeled as an SIMO system with the motor torque as the input and the hub angle and the tip position as the outputs. The two transfer functions are identified using a frequency-domain system identification method, and the resonant modes are determined. A feedback loop around the hub angle response with a resonant controller is designed to damp the resonant modes. A high-gain integral controller is also implemented to achieve zero steady-state error in the tip position response. Experiments are performed to demonstrate the effectiveness of the proposed control scheme.**

***Index Terms*—Flexible manipulator, integral controller, resonant controller, tip positioning.**

I. Introduction

INCREASING demands for high-speed manipulation and high payload-to-weight ratio in robot manipulators has triggered a significant growth in research and development activities on flexible manipulators. These manipulators constitute a suitable choice to realize such demands since they are light in weight, require only small-sized actuators and consume low energy for actuation [1]. However, designing feedback controllers to operate these systems at high speeds is a challenging task. The control system must be designed not only for precise tip positioning but also for suppressing vibrations associated with the flexible nature of the manipulator.

In order to achieve higher precision in the tip positioning, the use of tip position measurement is essential. In [2], Cannon and Schmitz initiated the experiment to control the tip positioning of a flexible manipulator by using measurements from a tip position sensor as a feedback input. They designed an linear qudratic Gaussian (LQG) controller and the obtained results suggested a satisfactory step response with accurate tip positioning. However, the LQG controller was not robust with respect to modeling errors. Since then many researchers, such as [3]–[8], have used the tip position measurement as feedback input to control the positioning of flexible manipulators.

In [6], the authors presented a two-feedback-loop control scheme to improve the closed-loop system robustness of the controller proposed in [2]. The controllers in the inner and outer loop were of LQG and H_∞ designs, respectively. The LQG controller was designed to introduce sufficient damping to the flexural modes and the H_∞ controller was designed for the purpose of increasing robustness and disturbance attenuation. Their simulation results illustrated an improvement in the closed-loop system robustness. However, the control scheme resulted in a high-order controller. A two-feedback-loop control scheme was also implemented by Feliu *et al.* in [4]. The inner and outer loops were used to control the motor position and tip position, respectively. In the outer loop, in contrast to [2], the motor position was used as the control signal instead of the current. As a result, the motor response needs to be significantly fast in order to counter the motion produced by the vibrational modes of the arm, making this method ineffective to suppress high-frequency vibrations. In [9] and [10], direct strain feedback (DSFB) control strategy was used to suppress the vibrations in a flexible manipulator. This control strategy managed to increase the stiffness of the flexible manipulator and caused it to undergo smaller vibration levels while in motion. It was noted in [9] that from a practical engineering perspective, this control strategy is only suitable for speed reference motor, where only the strain signal is needed for feedback. However, if a torque control motor is used, the time rate of change of strain, which is difficult to measure, is needed for feedback.

In this paper, an experimental flexible manipulator setup is fabricated to represent a typical flexible robotic arm. Frequency-domain system identification is used to model the flexible manipulator, and a control scheme is developed such that vibrations are suppressed using a collocated measurement while tip positioning is achieved using a noncollocated measurement. The control scheme consists of two feedback loops with each feedback loop having a specific purpose. The inner loop contains a resonant controller that adds damping to the flexible manipulator. It utilizes the hub angle measurement provided by a shaft encoder and guarantees that the closed-loop system remains stable in the presence of out-of-bandwidth dynamics, as described in [11] and [12]. In the outer loop, an integral controller is implemented for precise tip positioning using measurements of the tip deflection and hub angle. The integral controller ensures zero steady-state error for a step input.

Successful utilizations of resonant controllers for vibration suppression in flexible structures have been reported in [11] and [12]. This paper reports the first-time application of this control design approach to flexible manipulators. At the time of this writing, it is not known how an optimal resonant controller can be designed. This is mainly due to the nonconvex nature of the optimization problem associated with the minimization of a specific performance index. In this paper a graphical approach is proposed, which results in resonant controllers with satisfactory performance.

Manuscript received March 18, 2007; revised September 13, 2007. Recommended by Technical Editor S. Chiaverini. This work was supported by the Australian Research Council.

The authors are with the School of Electrical Engineering and Computer Science, University of Newcastle, Callaghan, NSW 2308, Australia (e-mail: iskandar.mahmood@newcastle.edu.au; reza.moheimani@newcastle.edu.au; bharath.bhikkaji@newcastle.edu.au).

Digital Object Identifier 10.1109/TMECH.2008.918494

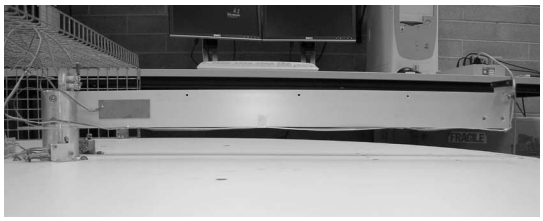

Fig. 1. Flexible manipulator.

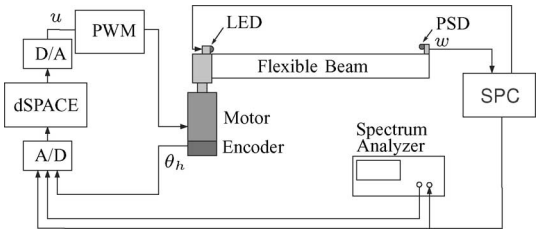

Fig. 2. Experimental setup for the flexible manipulator.

The remainder of the paper is arranged as follows. Section II provides a description of the experimental setup. Modeling and identification of the system transfer functions are presented in Section III. Control schemes are devised in Section IV. In Section V, simulation and experimental results are presented to illustrate the effectiveness of the proposed control schemes. Finally, conclusions are drawn in Section VI.

II. Experimental Setup

The flexible manipulator used here consists of an aluminum beam (0.6 m $\times$ 0.05 m $\times$ 0.003 m) clamped directly to the shaft of a Glentek GM4040-41 dc brush servo motor. An illustration of the experimental setup is presented in Figs. 1 and 2. The motor was driven by a Glentek GA377 pulse width modulation (PWM) servomotor amplifier. The motor has a continuous stall torque of 3.54 N·m and a maximum bandwidth of 58 Hz. The shaft encoder of the motor was used to measure the hub angle of rotation. It has a count of 5000 per revolution, i.e., a resolution of 0.072°.

An infrared light-emitting diode (LED) and a Hamamatsu S1352 position sensitive detector (PSD) were used for measuring the tip deflection of the beam. The LED was fixed on top of the hub. A Hamamatsu C5923 signal processing circuit (SPC) was used to drive the infrared LED and also to convert the photocurrents into a voltage signal, the magnitude of which is proportional to the spot light position on the sensor surface. A dSPACE DS1103 controller board was used for real-time controller implementation. A sampling frequency of 20 kHz was used in order to avoid aliasing.

III. Modeling and System Identification

In order to accurately model the system for control design, an experimental approach to modeling (system identification) is taken. The following frequency response functions (FRFs) are determined for designing the control system:

$$G_{\theta_h u}(\mathrm{i}\omega) \triangleq \frac{\theta_h(\mathrm{i}\omega)}{u(\mathrm{i}\omega)} \tag{1}$$

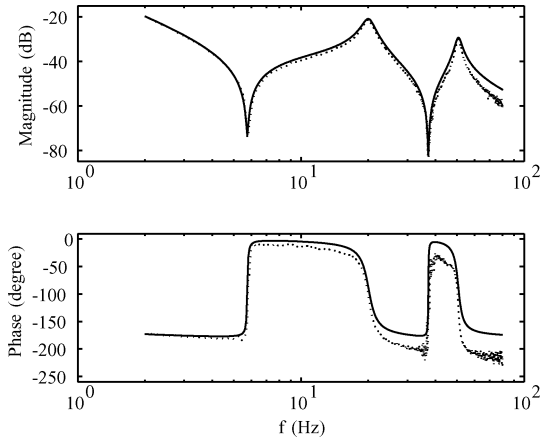

Fig. 3. Identified model (—) and experimental $(\cdots)$ frequency response of amplifier input voltage u to hub angle θ_h.

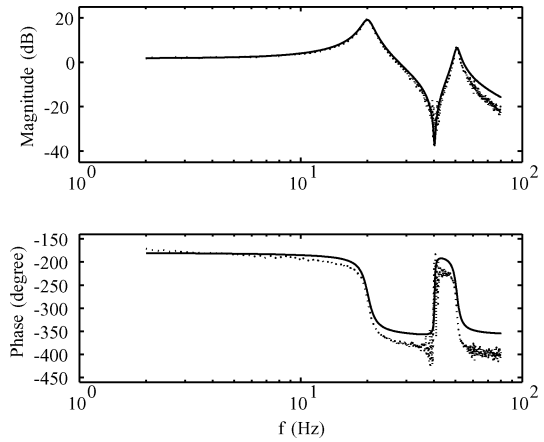

Fig. 4. Identified model (—) and experimental $(\cdots)$ frequency response of amplifier input voltage u to tip deflection w_{tip}.

and

$$G_{w_{\mathrm{tip}} u}(\mathrm{i}\omega) \triangleq \frac{w_{\mathrm{tip}}(\mathrm{i}\omega)}{u(\mathrm{i}\omega)} \tag{2}$$

where $u(t)$ is the input voltage, $\theta_h(t)$ is the hub angle measured by the shaft encoder, $w_{\mathrm{tip}}(t) = w(L,t)$ is the flexural tip deflection measured by the PSD. It is worth noting that the tip position $y_{\mathrm{tip}}(t) \triangleq y(L,t)$ can be described by $y(L,t) = w(L,t) + L\theta_h(t)$, which leads to the expression

$$G_{y_{\mathrm{tip}} u}(\mathrm{i}\omega) = G_{w_{\mathrm{tip}} u}(\mathrm{i}\omega) + L G_{\theta_h u}(\mathrm{i}\omega). \tag{3}$$

A dual-channel HP35670A spectrum analyzer was used for determining the FRFs. A band-limited random noise signal (2–102 Hz) was generated using the spectrum analyzer and applied to the motor as the input, $u(t)$. The corresponding outputs $\theta_h(t)$ and $w_{\mathrm{tip}}(t)$ were also recorded using the spectrum analyzer. The input–output data was processed to generate the FRFs (1) and (2) in a nonparametric form. In Figs. 3 and 4 the nonparametric FRFs of (1) and (2) are plotted along with the corresponding

parametric fits

$$G_{\theta_h u}(s) = \frac{420.73\left(s^2 + 0.5028s + 1305\right)}{s\left(s + 1.65\right)s^2 + 15.35s + 1.596 \times 10^4} \times \frac{s^2 + 1.437s + 5.462 \times 10^4}{s^2 + 20.9s + 1.015 \times 10^5} \quad (4)$$

and

$$G_{w_{\text{tip}} u}(s) = \frac{-31153.01}{s^2 + 15.35s + 1.596 \times 10^4} \times \frac{s^2 + 3.108s + 6.386 \times 10^4}{s^2 + 20.9s + 1.015 \times 10^5}. \quad (5)$$

Note that the poles characterizing flexible modes of the beam in $G_{\theta_h u}(s)$ and $G_{w_{\text{tip}} u}(s)$ are identical. This property is common to all flexible structures. Data beyond 80 Hz were discarded in Figs. 3 and 4 as these frequencies were far beyond the maximum bandwidth of the motor. Fig. 3 illustrates the collocated nature of $G_{\theta_h u}(s)$, where the phase is always between 0° and -180°.

IV. Controller Design

This section discusses and details the control design scheme proposed in this paper. The control scheme consists of two negative feedback loops. The inner loop is designed to add damping to the flexible manipulator and the outer loop provides precise tip positioning.

A. Resonant Controller Design (Inner Loop Controllers)

Feedback controllers that increase the effective damping and at the same time guarantee unconditional stability of the closed-loop system are always preferred since they avoid closed-loop instabilities due to spillover effects [13]. It is known that collocated velocity feedback controllers [13] possess such properties. However, the implementation of this controller requires the realization of a differentiator, which is not possible for systems with large bandwidth. Another drawback of the velocity feedback controller is that it results in a high control effort over all frequencies. Ideally, for vibration damping purposes, the control effort should be restricted to the resonance frequencies only. Resonant controllers are a class of feedback controllers that guarantee unconditional closed-loop stability of collocated systems, [11], [14]. The model structure of resonant controllers is such that they approximate a differentiator over a narrow bandwidth around the resonance frequencies of the structure. The motivations for their model structure comes from passive RL network controllers used for piezoelectric shunt damping, see [15] and [16]. A detailed discussion on the connections between passive RL network controllers and resonant controllers can be found in [17].

As the poles characterizing the flexible modes of $G_{\theta_h u}(s)$ and $G_{y_{\text{tip}} u}(s)$ are identical, system resonances can be damped by designing a feedback loop around either $G_{\theta_h u}(s)$ or $G_{y_{\text{tip}} u}(s)$. Here, $G_{\theta_h u}(s)$ is chosen as its collocated nature guarantees an unconditional closed-loop stability with resonant controllers. Damping can be achieved by shifting the closed-loop poles of $G_{\theta_h u}(s)$ deeper into the left-half plane (LHP).

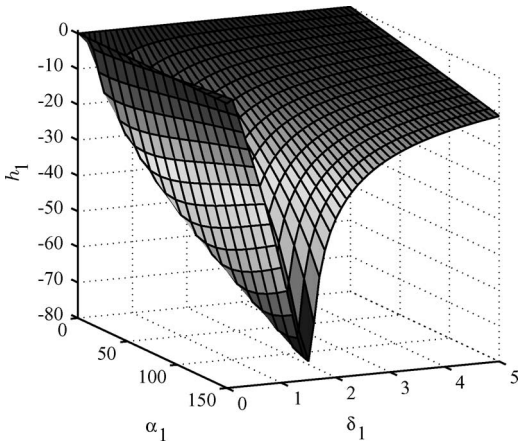

Fig. 5. Plot of the distance between the open-loop and closed-loop poles h_1 versus α_1 and δ_1, for the first flexible mode.

In the current context, the resonant controller can be parameterized as

$$K^\alpha(s) = \sum_{i=1}^{N} \frac{\alpha_i s^2}{s^2 + 2\delta_i \omega_i s + \omega_i^2} \quad (6)$$

where $\alpha_i, \beta_i, \delta_i$, and ω_i are the design parameters and N is the number of modes that need to be controlled [12]. As only the first two resonant modes are considered, N is set to 2, which implies

$$K^\alpha(s) = K_1^\alpha(s) + K_2^\alpha(s) \quad (7)$$

where

$$K_i^\alpha(s) = \frac{\alpha_i s^2}{s^2 + 2\delta_i \omega_i s + \omega_i^2}, \quad i = 1, 2. \quad (8)$$

As mentioned in Section I, an optimal resonant controller design has not yet been reported. The approach taken here to determine the parameters is similar to the one mentioned in [11], where each resonant filter is determined independently. It is possible to do so since interactions of the resonant filters are marginally coupled. As the filters $K_1^\alpha(s)$ and $K_2^\alpha(s)$ are targeted to damp the first and the second resonant modes of the plant, the values of ω_1 and ω_2 are set to the first and second resonance frequencies of the beam, respectively. In order to determine the other parameters, the following method is adopted. Assume that only $K_1^\alpha(s)$ exists in the feedback loop. The values of α_1 and δ_1 are chosen such that the absolute value of the difference h_1 between the real parts of the open-loop and closed-loop poles corresponding to the first resonant mode is maximized. Fig. 5(a) shows that for a given range of α_1 ($0 \leq \alpha_1 \leq 150$), there exists a value of δ_1 that maximizes the absolute value of h_1. Similarly to determine α_2 and δ_2, it is assumed that the filter $K_1^\alpha(s)$ is not part of the feedback loop and α_2 and δ_2 are chosen such that the difference h_2, between the real parts of the open-loop and closed-loop poles corresponding to the second resonant mode, is maximized. Fig. 5(b) illustrates that for a given range of α_2 ($0 \leq \alpha_i \leq 150$), there exists a value of δ_2 that maximizes the absolute value of h_2. The controller obtained by using the

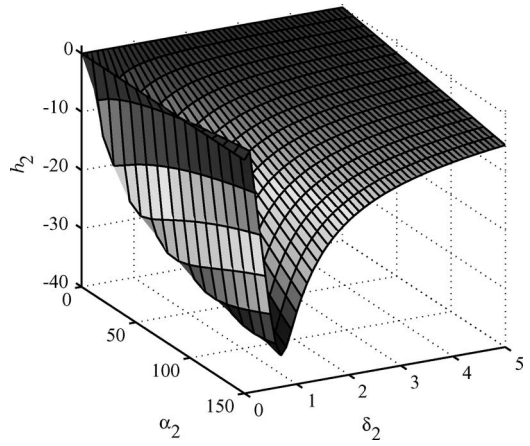

Fig. 6. Plot of the distance between the open-loop and closed-loop poles h_2 versus α_2 and δ_2, for the second flexible mode.

aforesaid method is

$$K^{\alpha}(s) = \frac{150s^2}{s^2 + 378.3s + 1.59 \times 10^4} + \frac{150s^2}{s^2 + 445.8s + 1.014 \times 10^5}. \quad (9)$$

Note that in closed loop, the resonant controller $K^{\alpha}(s)$ will not shift the pole located at the origin. This can be seen by setting $G_{\theta_h u}(s) = a(s)/sb(s)$, $G_{y_{\rm tip} u}(s) = m(s)/sb(s)$, and $K^{\alpha}(s) = s^2 p(s)/q(s)$, where $a(s), b(s), m(s), p(s)$, and $q(s)$ are appropriately defined, and noting that

$$G^{(cl)}_{\theta_h u_\circ}(s) = \frac{G_{\theta_h u}(s)}{1 + K^{\alpha}(s) G_{\theta_h u}(s)} = \frac{1}{s}\left(\frac{a(s)q(s)}{q(s)b(s) + sp(s)a(s)}\right) \quad (10)$$

and

$$G^{(cl)}_{y_{\rm tip} u_\circ}(s) = \frac{G_{y_{\rm tip} u}(s)}{1 + K^{\alpha}(s) G_{\theta_h u}(s)} = \frac{1}{s}\left(\frac{m(s)q(s)}{q(s)b(s) + sp(s)a(s)}\right). \quad (11)$$

B. Outer Loop for Positioning

Here, an integral controller $K_{\rm Int} = K_I/s$ is designed for the outer feedback loop to achieve precise tip positioning. The controller is designed such that the tip response to a step input would satisfy the following specifications: 1) zero steady-state tip position error, 2) rise time and settling time of less than 1 and 1.5 seconds, respectively; and 3) overshoot of less than 2%. However, direct application of an integral controller to $G^{(cl)}_{y_{\rm tip} u_\circ}(s)$ can be problematic (11). This can be verified by observing the root locus of the net closed-loop tip response

$$\frac{K_I/s\, G^{(cl)}_{y_{\rm tip} u_\circ}(s)}{1 + K_I/s\, G^{(cl)}_{y_{\rm tip} u_\circ}(s)} \quad (12)$$

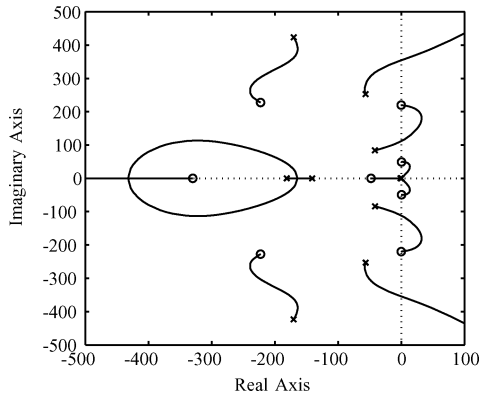

Fig. 7. Roots locus for $G_{y_{\rm tip} u}(s)$ with resonant controller $K^{\alpha}(s)$ and integral controller K_I/s in the feedback loops, as K_I increases.

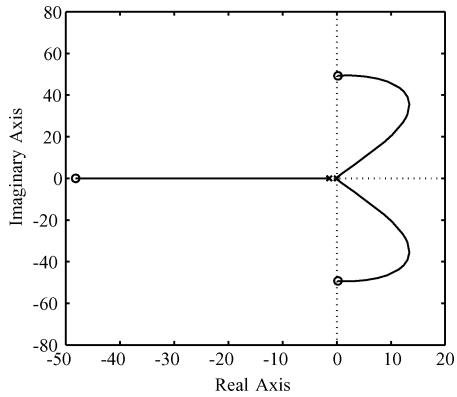

Fig. 8. Enlarged roots locus for $G_{y_{\rm tip} u}(s)$ with resonant controller $K^{\alpha}(s)$ and integral controller K_I/s in the feedback loops, as K_I increases.

obtained by varying K_I. The locus plot is presented in Fig. 7(a) and shows that for any $K_I \geq 0$, the closed-loop transfer function (12) is unstable. In Fig. 7(b), an enlarged version of Fig. 7(a) around the origin is presented. It shows two locus paths starting from the origin and lying entirely in the right-half plane (RHP) thereafter, demonstrating instability.

A standard way to correct this problem is to add a compensator $C(s)$ to the resonant controller, *i.e.*, replace the resonant controller $K^{\alpha}(s)$ by $K_a(s) = K^{\alpha}(s) + C(s)$, so that the pole at the origin is shifted into the LHP; see Fig. 9 for an illustration. In order to avoid a large increase in the model order of the controller and, at the same time push the pole at the origin well into the LHP, a phase-lead compensator, $C(s) = K_{pl}(s+z)/(s+p)$ where K_{pl}, z, and p are the design parameters, is used. Here, the parameters are determined through pole placement, following guidelines in [18, Ch. 10]. Here we set the compensator, $C(s) = 70(s+10)/s + 70$, which implies that the augmented resonant controller is equal to

$$K_a(s) = \frac{70(s+10)}{s+70} + \frac{150s^2}{s^2 + 378.3s + 1.59 \times 10^4} + \frac{150s^2}{s^2 + 445.8s + 1.014 \times 10^5}. \quad (13)$$

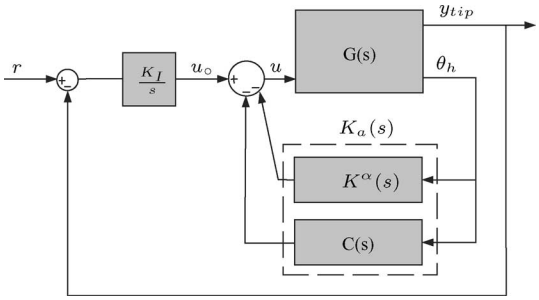

Fig. 9. Augmented resonant controller $K_a(s)$ and integral controller.

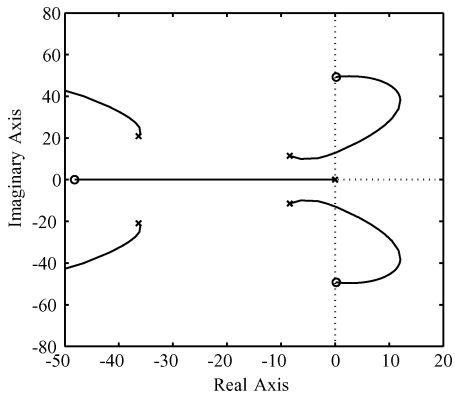

Fig. 10. Enlarged roots locus for $G_{y_{\rm tip}u}(s)$ with augmented resonant controller $K_a(s)$ and integral controller in the feedback loops, as K_I is varied.

Fig. 10 shows an enlarged root locus of (12) with $K^\alpha(s)$ replaced by $K_a(s)$. It can be seen that by shifting the system pole at the origin into the LHP, some parts of the two locus paths are in the LHP, allowing for some values of K_I to result in a stable closed-loop system.

V. Simulations and Experimental Results

This section presents simulation and experimental results obtained from the control scheme proposed in this paper.

A. Resonant and Integral Controller

The performance of the augmented resonant controller $K_a(s)$ was evaluated first. Fig. 11 shows the simulated and measured closed-loop frequency responses of $G_{\theta_h u}(s)$. It is evident that the experimental results match the simulations except near the second resonant mode. This is due to the fact that the second resonance is very close to the maximum bandwidth of the motor. The frequency range of the simulated frequency response was extended to cover 1–100 Hz range to illustrate that the pole at $s = 0$ has been shifted to the left by the phase-lead compensator.

In Fig. 12, experimentally determined closed-loop frequency responses of $G_{\theta_h u}(s)$ and $G_{w_{\rm tip}u}(s)$ are plotted along with their corresponding open-loop frequency responses. A significant damping in the first and the second resonances of both $G_{\theta_h u}(s)$ and $G_{w_{\rm tip}u}(s)$ is evident from the plots. In particular, Fig. 12(a) illustrates 20 and 19 dB damping on the first and second resonant modes of $G_{\theta_h u}(s)$, respectively. Furthermore,

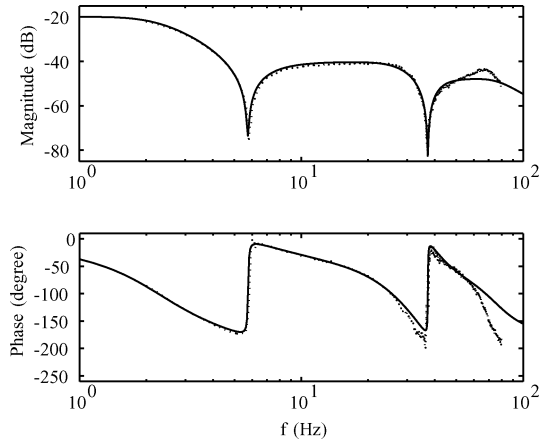

Fig. 11. Simulated (—) and experimental $(\cdots)$ closed-loop frequency responses of amplifier input voltage u to hub angle θ_h using augmented resonant controller $K_a(s)$.

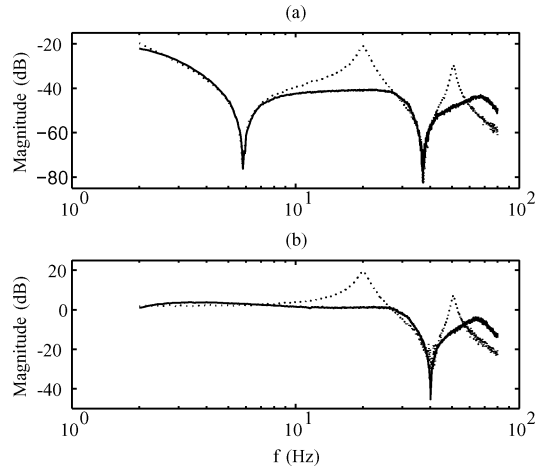

Fig. 12. Open-loop $(\cdots)$ and closed-loop (—). Frequency responses using augmented resonant controller $K_a(s)$. (a) Amplifier input voltage u to hub angle θ_h. (b) Amplifier input voltage u to tip deflection $w_{\rm tip}$.

Fig. 12(b) shows damping of 18 dB on the first and second resonant modes of $G_{w_{\rm tip}u}(s)$.

Having the flexible manipulator significantly damped by the resonant controller, experiments were performed to slew the tip to a set point $y_{\rm tip} = \pi L/4$ m, with the initial position being set to zero. Initially, the tip was slewed in open-loop to obtain the open loop time response of the tip position and tip deflection. The amount of time taken and the input voltage u needed to be applied to the motor in order to slew the tip to the set point was determined through simulation. Fig. 13 illustrates that the open-loop control resulted in a tip position response with a large steady-state error, long rise and settling times, and a highly oscillating tip.

Similar slewing experiments were performed with an integral controller in the outer feedback loop. Here, the root locus approach was used in selecting the integral controller gain K_I, such that the tip response of the flexible manipulator satisfied the necessary specifications. Fig. 14(a) shows the closed-loop time response of tip position $y_{\rm tip}$ with $K_I = 30$. It is apparent

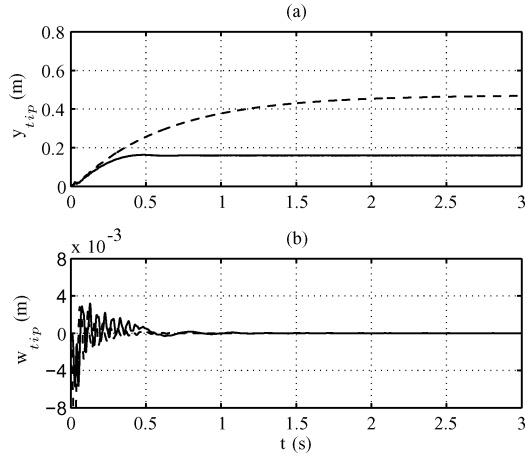

Fig. 13. Experimental (—) and simulated $(--)$. Time response of (a) tip position $y_{\rm tip}$ and (b) tip deflection $w_{\rm tip}$, in open loop.

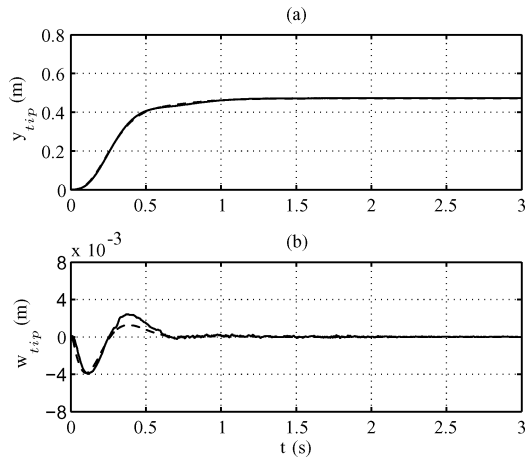

Fig. 14. Experimental (—) and simulation $(--)$. Time response of (a) tip position $y_{\rm tip}$ and (b) tip deflection $w_{\rm tip}$, using augmented resonant controller $K_a(s)$ and integral controller for $K_I = 30$.

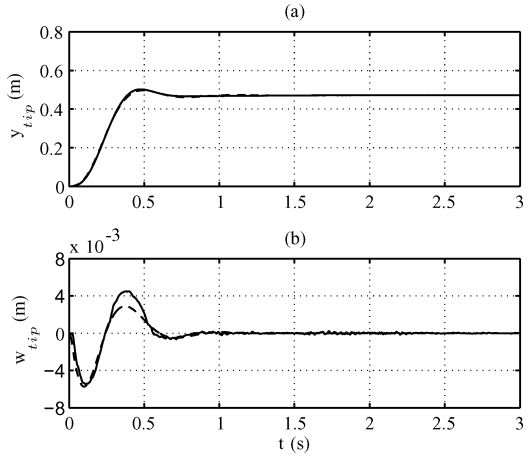

Fig. 15. Experimental (—) and simulation $(--)$. Time response of (a) tip position $y_{\rm tip}$ and (b) tip deflection $w_{\rm tip}$, using augmented resonant controller $K_a(s)$ and integral controller for $K_I = 45$.

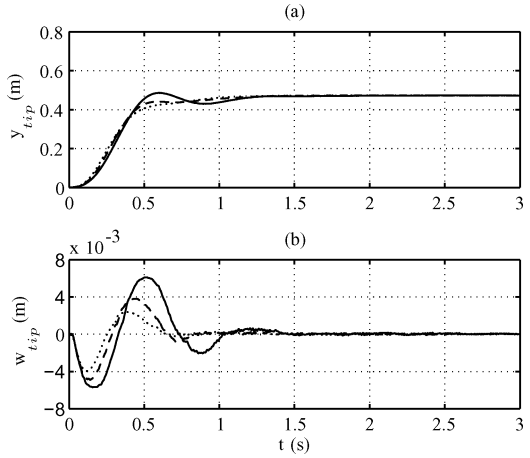

Fig. 16. Time response of (a) tip position $y_{\rm tip}$ and (b) Tip deflection $w_{\rm tip}$, using augmented resonant controller $K_a(s)$ and integral controller with tip mass = 92 g (—), tip mass = 35 g $(--)$, and no mass $(\ldots)$.

from the plot that $y_{\rm tip}$ has a zero steady-state error, a zero overshoot, a rise time of 0.5 s, and a settling time of 1.0 s. The high gain in K_I has allowed the tip position to have zero steady-state error in 1.3 s. Fig. 14(b) illustrates that the resonant controller completely suppresses the tip vibrations during, and at the end of the slewing maneuver.

A faster response of $y_{\rm tip}$ can be obtained by increasing the K_I, but this comes at the expense of a higher overshoot. Fig. 15(a) shows the response $y_{\rm tip}$ when K_I is increased to 45. The rise and settling times have decreased to 0.2 and 0.6 s, respectively, while the overshoot has increased from 0 to 6.6%. It is worth noting that, even for a faster tip position response, Fig. 15(b) does not show any indication of tip vibrations.

B. Illustration of Robustness

The first robustness test was performed by attaching a certain amount of mass to the tip to alter the dynamics and natural frequencies of the flexible manipulator. This test is performed to study closed-loop performance of the controller with a change in payload. Two masses are used here; the first has a weight of 35 g (which is 14% of the flexible beam weight) and a second one has a weight of 92 g (which is 35% of the flexible beam weight). With these masses at the tip, no elevation in the tip vibrations was observed, but there was a small overshoot in the $y_{\rm tip}$ response (Fig. 16). However, the overshoot is still within the given specifications.

The second robustness test was performed against the size of input commands. Fig. 17 demonstrates no loss of performance in the $y_{\rm tip}$ and $w_{\rm tip}$ responses when the larger input command of $\pi L/2$ m was used. The $y_{\rm tip}$ response still has similar rise time, settling time, and overshoot regardless of the larger input command.

VI. Conclusion

In this paper, frequency-domain system identification was used to model a single-link flexible manipulator. The identified models have accurately predicted the frequency and time responses of the flexible manipulator in open and closed loop.

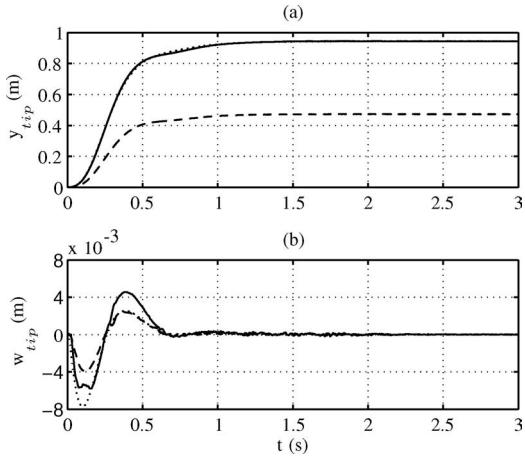

Fig. 17. Time response of (a) tip position $y_{\rm tip}$ and (b) tip deflection $w_{\rm tip}$, using augmented resonant controller $K_a(s)$ and integral controller for large-step input command, $\pi L/2$ m experimental (—), simulation $(\cdots)$ and for small-step input command $\pi L/4$ $(--)$ m.

The transfer functions characterizing the collocated hub angle $\theta_h(t)$ response to the input $u(t)$ and the noncollocated tip position $y_{\rm tip}(t)$ response to the input $u(t)$ were found to have the same dynamic modes. This allows for the damping of the tip position $y_{\rm tip}(t)$ response, indirectly, by damping the collocated hub angle $\theta_h(t)$ response. A resonant controller was designed to damp the highly resonant modes of the flexible manipulator. The resonant controller performed successfully in damping those modes. The resonant controller was also augmented with a phase-lead compensator to enable it to be used with a high-gain integral controller to achieve precise tip positioning. It was also found that the proposed control scheme was robust to perturbations in the resonance frequencies of the flexible manipulator and the size of the input command.

REFERENCES

[1] A. R. Fraser and R. W. Daniel, *Perturbation Techniques for Flexible Manipulators*. Norwell, MA: Kluwer, 1991.

[2] R. H. Cannon and E. Schmitz, "Initial experiments on the end-point control of a flexible one-link robot," *Int. J. Robot. Res.*, vol. 3, no. 3, pp. 62–75, 1984.

[3] W. T. Qian and C. C. H. Ma, "A new controller design for a flexible one-link manipulator," *IEEE Trans. Autom. Control*, vol. 37, no. 1, pp. 132–137, Jan. 1992.

[4] V. Feliu, K. S. Rattan, and H. B. Brown, "Control of flexible arms with friction in the joints," *IEEE Trans. Robot. Autom.*, vol. 9, no. 4, pp. 467–475, Aug. 1993.

[5] J.-H. Park and H. Asada, "Dynamic analysis of noncollocated flexible arms and design of torque transmission mechanisms," *J. Dyn. Syst., Meas., Control*, vol. 116, pp. 201–207, 1994.

[6] R. N. Banavar and P. Dominic, "An LQG/H_∞ controller for a flexible manipulator," *IEEE Trans. Control Syst. Technol.*, vol. 3, no. 4, pp. 409–416, Dec. 1995.

[7] H. Krishnan and M. Vidyasagar, "Control of single-link flexible beam using hankel-norm-based reduced-order model," *Proc. Inst. Elect. Eng. Control Theory Appl.*, vol. 145, no. 2, pp. 151–158, Mar. 1998.

[8] M.-T. Ho and Y.-W. Tu, "Position control of a single-link flexible manipulaotr using H_∞-based PID control," *Proc. Inst. Elect. Eng.—Control Theory Appl.*, vol. 153, no. 5, pp. 615–622, Sep. 2006.

[9] Z.-H. Luo, "Direct strain feedback control of flexible robot arms: New theoretical and experimental results," *IEEE Trans. Autom. Control*, vol. 38, no. 11, pp. 1610–1622, Nov. 1993.

[10] S. S. Ge, T. H. Lee, and G. Zhu, "Improving regulation of a single-link flexible manipulator with strain feedback," *IEEE Trans. Robot. Autom.*, vol. 14, no. 14, pp. 179–185, Feb. 1998.

[11] H. R. Pota, S. O. R. Moheimani, and M. Smith, "Resonant controllers for smart structures," *Smart Mater. Struct.*, vol. 11, no. 1, pp. 1–8, 2002.

[12] S. O. R. Moheimani and B. J. G. Vautier, "Resonant control of structural vibration using charge-driven piezoelectric actuators," *IEEE Trans. Control Syst. Technol.*, vol. 13, no. 6, pp. 1021–1035, Nov. 2005.

[13] M. J. Balas, "Feedback control of flexible structures," *IEEE Trans. Autom. Control*, vol. 23, no. 4, pp. 673–679, Aug. 1978.

[14] D. Halim and S. O. R. Moheimani, "Spatial resonant control of flexible structures—Application to a piezoelectric laminate beam," *IEEE Trans. Control Syst. Technol.*, vol. 9, no. 1, pp. 37–53, Jan. 2001.

[15] N. W. Hagood, W. H. Chung, and A. v. Flotow, "Modelling of piezoelectric actuator dynamics for active structural control," *J. Intell. Mater. Syst. Struct.*, vol. 21, no. 3, pp. 327–354, 1990.

[16] K. W. Wang *Structural Vibration Suppression Via Parametric Control Actions—Piezoelectric Materials With Real-Time Semi-Active Networks*, A. Guran and D. J. Inman, Eds. , Singapore: World Scientific, 1995.

[17] S. O. R. Moheimani, A. J. Fleming, and S. Behrens, "On the feedback structure of wideband piezoelectric shunt damping systems," *Smart Mater. Struct.*, vol. 12, pp. 49–56, Feb. 2003.

[18] R. C. Dorf and R. H. Bishop, *Modern Control Systems*. Reading, MA: Addison-Wesley, 1998.

Iskandar A. Mahmood was born in Malaysia in 1975. He received the B. Eng. and M.Sc. degrees in mechatronics engineering from the International Islamic University Malaysia, Kuala Lumpur, Malaysia, in 1999 and 2004, respectively. He is currently working toward the Ph.D. degree in electrical engineering at the University of Newcastle, Callaghan, Australia.

Since 2005, he has been with the Laboratory of Dynamics and Control of Nanosystems, University of Newcastle.

S. O. Reza Moheimani (SM'01) received the Ph.D. degree in electrical engineering from the University of New South Wales at Australian Defence Force Academy, Canberra, Australia, in 1996.

Since 1997, he has been with the University of Newcastle, Callaghan, Australia, where he is a Professor with the School of Electrical Engineering and Computer Science. He also serves as the Assistant Dean (Research) for the Faculty of Engineering, and an Associate Director of the Centre for Complex Dynamic Systems and Control, an Australian Government Centre of Excellence. He has published two books, several edited volumes, and over 150 refereed articles. His current interests include applications of control and estimation in nanoscale positioning systems for scanning probe microscopy, control of electrostatic micro-actuators in MEMS, and data storage systems.

Prof. Moheimani is a recipient of the 2007 IEEE TRANSACTIONS ON CONTROL SYSTEMS TECHNOLOGY Outstanding Paper Award, and a Fellow of the Institute of Physics, U.K. He is an Associate Editor of several international journals, and has chaired a number of international workshops and conferences.

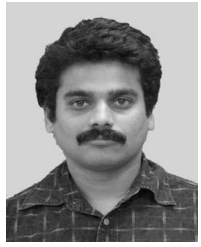

Bharath Bhikkaji received the Ph.D. degree in signal processing from Uppsala University, Uppsala, Sweden, in 2004.

He is currently a Research Academic in the School of Electrical Engineering and Computer Science, University of Newcastle, Callaghan, Australia. His current research interests include system identification, robust control, and active noise and vibration control of flexible structures.